Ceramics International 43 (2017) 6039–6047

Contents lists available at ScienceDirect

Ceramics International

journal homepage: www.elsevier.com/locate/ceramint

Sodium carbonate activated slag as cement replacement in autoclaved aerated concrete

B. Yuan[a,b,1], C. Straub[b,c,1], S. Segers[b], Q.L. Yu[b,*], H.J.H. Brouwers[a,b]

[a] State Key Laboratory of Silicate Materials for Architectures, Wuhan University of Technology, Wuhan 430070, PR China
[b] Department of the Built Environment, Eindhoven University of Technology, P.O. Box 513, 5600 MB Eindhoven, The Netherlands
[c] Materials Innovation Institute, P.O. Box 5008, 2600 GA Delft, The Netherlands

ARTICLE INFO

Keywords:
Autoclaved aerated concrete
Sodium carbonate activated slag
Reaction product
Microstructure
Compressive strength
Environmental impact

ABSTRACT

This paper aims to study the suitability of fully replacing cement by sodium carbonate activated slag in producing autoclaved aerated concrete (AAC). The material properties of the product are characterized in terms of green strength development, mechanical properties, pore related properties such as porosity and thermal conductivity, shrinkage and reaction products. The produced alkali-activated slag-based AAC (ASAAC) shows comparable material properties to the designed cement-based reference AAC samples by giving a compressive strength of −25% with raw density of +18%, thermal conductivity of +13% with a porosity of −5% and drying shrinkage of +5.5%. Besides, a relatively higher crystallinity of calcium silicate hydrates and Al incorporation in the chain of C-S-H is observed for ASAAC products. Furthermore, significant reductions in cost, energy consumption and CO_2 emission are foreseen.

1. Introduction

Autoclaved aerated concrete (AAC) has shown many advantages in terms of low thermal conductivity, low density, low shrinkage and good fire resistance [1–6], etc. In general, the raw materials are cement, lime, gypsum, quartz sand and metallic Al powder (forming hydrogen gas) and the porosity of AAC is around 80% [1,7]. To make this product more sustainable and environmentally friendly, extensive attentions have been paid to the replacement of raw materials with different wastes: skarn-type copper tailings and blast furnace slag fully replacing lime [8], rice husk ash as partial replacement for fine aggregate [9], fly ash replacing quartz [2] or acting as secondary raw material substituting lime and sulfate [10], coal bottom ash [11] or self-ignition coal gangue using as an aggregate [12], etc. However, attempts on fully replacing cement in AAC production are rarely reported.

Alkali activated materials (AAM) have been of great interest to the academic field over the last decades and are showing superiorities concerning strength development, durability and environmental benefits [13]. The concept of AAM is using alkaline solution to activate the reactivity of industrial by-products in order to obtain a sustainable building material. It is noteworthy that the properties of AAC are dominated by the pores, including type, shape, size and distributions, etc. Thus, the formation of hydrogen gas (Eq. (1)) is crucial to the material properties. In general, the pH of AAM (≈14) is higher than that of cement materials (mainly based on $Ca(OH)_2$ having a pH of ≈12.5), leading to a faster reaction as the pH is the main driving force:

$$2Al + 2OH^- + 6H_2O \Rightarrow 2[Al(OH)_4]^- + 3H_2 \uparrow . \quad (1)$$

However, an accelerated release of H_2 may not be beneficial for the porosity development. Nevertheless, because of the generally high viscosity and fast setting of AAM, the hydrogen gas can still be effectively entrapped in the matrix, indicating that the AAM can be suitable for the production of AAC in fully replacing cement. As of today, only a few studies have investigated the possibilities of producing geopolymer foam concrete [14–16] or non-autoclaved high strength cellular concrete from alkali activated slag [17]. However, the production and properties of foam concrete is different from AAC, though both of them are categorized cellular concrete [7]. Furthermore, only waterglass modified with sodium hydroxide was used as activators in these studies. In principle, the materials properties of AAM are determined by the raw materials and activators [18–22]. It is reasonable to apply NaOH modified waterglass as the activator as it provides a very good activation effect with regard to mechanical properties and durability [23–26]. However, the problems of fast setting, temperature sensitive and high shrinkage limit the practical application of this activator [27–30]. Besides, waterglass is commonly produced by

* Corresponding author.
E-mail address: q.yu@bwk.tue.nl (Q.L. Yu).
[1] The equivalent first authors.

http://dx.doi.org/10.1016/j.ceramint.2017.01.144
Received 18 November 2016; Received in revised form 10 January 2017; Accepted 30 January 2017
Available online 01 February 2017
0272-8842/ © 2017 Elsevier Ltd and Techna Group S.r.l. All rights reserved.

Table 1
Chemical compositions of the raw materials.

Chemical compositions	Quartz	Anhydrite	Cement	Portlandite[a]	Lime[c]	GGBS
Na_2O+K_2O	0.05	0.37	1.08	0.11	0.27	0.64
MgO	–	1.20	0.96	0.33	0.58	9.49
Al_2O_3	0.85	0.65	4.88	0.13	0.40	12.92
SiO_2	98.6	1.55	15.7	0.30	0.67	30.52
SO_3	–	53.7	3.98	0.05	0.03	3.48
CaO	0.01	38.9	66.5	70.1	95.9	40.35
Fe_2O_3	0.03	0.19	2.48	0.17	0.26	0.56
L.O.I.	0.26	3.08[b]	2.38	27.4	1.81	−0.35
True density [kg/m³]	2570	2950	3120	2300	3240	2920

[a] Calcite content ≈15% (det. by LOI and density).
[b] The L.O.I of anhydrite was measured at 650 °C.
[c] Portlandite content ≈10% (det. by LOI and density), Slaking lime test (EN 459-2): $t_{60\ °C}$=10 min/T_{max}=75.8 °C.

roasting soda ash (Na_2CO_3) and silica sand in a furnace at temperatures between about 1000 and 1400 °C, which involves high energy consumption and greenhouse gas emission [31].

On the other hand, sodium carbonate activation has been reported to possess good performance in terms of material properties, cost-effectiveness and sustainability [32,33]. Moreover, though the pH of the sodium carbonate solution is low (10–11) compared to that of $Ca(OH)_2$ (≈12.5), the pH of the mixture will quickly develop to ≈14 due to the presence of lime following the reaction:

$$Na_2CO_3 + Ca(OH)_2 \Rightarrow 2NaOH + CaCO_3 \downarrow . \quad (2)$$

In this case, sodium carbonate activation is switched to sodium hydroxide activation, while the presence of fine quartz provides extra silicate, enabling a similar effect as waterglass modification. The utilization of cement in the AAC system is mainly for providing sufficient green strength for the demoulding and transporting of samples for further curing. Slow reaction of sodium carbonate activated slag has been often reported [18,34]. However, by adding chemical additives (NaOH [35,36], waterglass [33] or calcined layered double hydroxides [37]), blending with reactive admixtures (MgO [38] and lime [39,40]) or changing the fineness of slags, the reaction can be significantly accelerated to meet the requirements of the green strength development of AAC. As lime is present in the mixture, the problem of slow sodium carbonate activation is overcome. In this case, sodium carbonate activation is preferable for the production of AAC by totally substituting the cement. In fact, sodium carbonate was used as accelerator in producing AAC [4] and slag as quartz replacement in the patent of Eriksson [41].

In this study, sodium carbonate activated slag was investigated as an alternative binder to cement to design autoclaved aerated concrete, with the aim to evaluate the methodology and the general principle of a cement-free alkali activates AAC. The target flowability was firstly determined by preliminary experiments and then the selected mixture was prepared on a large scale and characterized in terms of fresh state behaviour (green body development), hardened state properties (mechanical properties, microstructure, porosity, shrinkage and thermal conductivity), and reaction products. In addition, the influence of sodium carbonate dosage on the microstructure change of ASAAC was studied. Furthermore, life cycle assessment with respect to cost, energy consumption and CO_2 emission of cement and sodium carbonate activated slag was performed.

2. Materials and experiment

2.1. Materials

All materials used for preparing the samples are technical grade and, if not indicated otherwise, fulfil the recommended requirements for AAC production [1,2,7,35,42] or originated from AAC material suppliers, except ground granulated blast furnace slags (GGBS) (provided by ENCI B.V, the Netherlands) (Table 1). All experiments follow a sand-based reference recipe (provided by HESS AAC Systems B.V., Table 2). The chemical compositions of the raw materials were measured by X-ray Fluorescence (XRF, PANalytical Epsilon3) with pressed powder tablets and the particle size distributions were obtained by a laser granulometer (Malvern Mastersizer 2000), as shown in Table 1 and Fig. 1, respectively. The basicity coefficient (K_b=CaO+MgO/SiO_2+Al_2O_3) of GGBS was 1.3. The true density of the powders was determined by using a helium pycnometer (Micromeritics AccuPyc II 1340).

2.2. Sample preparation

For the preparation of the reference mixture (AAC), the experiments were performed as follows: after preheating the specific water amount (dependent on the water-to-powder-ratio, W/P ratio) to 45 °C, it was put in the mixer (A Swinko EZR 22R, R/L with a 4-bladed

Table 2
Mix proportions of the raw materials for AAC and ASAAC (kg/batch).

Mix proportions	Ref. (AAC)	ASAAC
CEM I 42.5R	2.4	–
GGBFS	–	2.175
Na_2CO_3	–	0.225
CaO	1	1
$Ca(OH)_2$	0.3	0.3
SiO_2	8	8
$CaSO_4$	0.3	0.3
H_2O	7.5	8.4
Al Powder	0.01	0.01
W/P	0.625	0.7

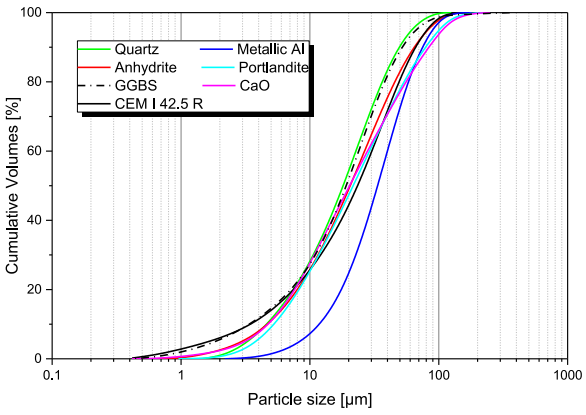

Fig. 1. Particle size distributions of the raw materials.

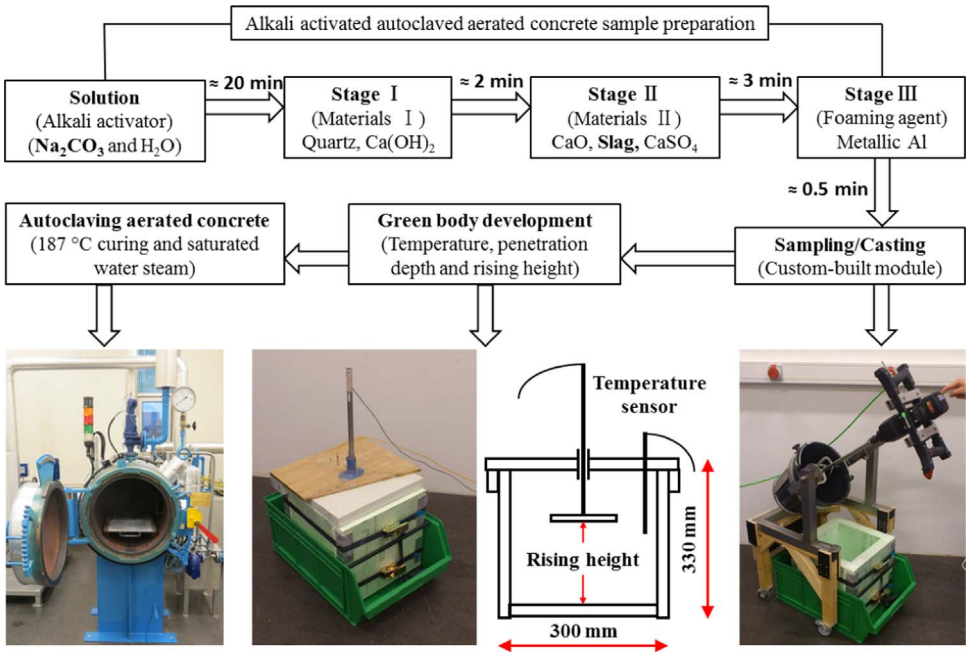

Fig. 2. Scheme of preparing alkali activated autoclaved aerated concrete (ASAAC). (For interpretation of the references to color in this figure, the reader is referred to the web version of this article).

propeller mixing rod) and stirred at a slow speed. Separately, the aluminium powder (Benda-Lutz® 5-6380 from Benda-Lutz Skawina Sp. z o. o./SunChemical) was manually pre-dispersed in water: A small part of the mixing water (≈100 ml) was separated. The Al powder and half of the water were mixed in a closed container by strong shaking (with a tiny droplet of surfactant). Quartz and portlandite were successively added and mixed for minimum 60 s, in order to ensure homogeneity. The addition of lime (time=0), cement and anhydrite (after 30 s) was performed and then the mixing was continued for 90 s. Finally the aluminium powder suspension was added (and the container is rinsed out with the remaining separated water to ensure that all Al powder is utilized and the W/S ratio is correct). As for the preparation of AAAC, a slightly different procedure was applied as shown in Fig. 2.

The samples were demoulded on the following day (after about 12 h) and placed directly in the autoclave of our lab (autoclave: Maschinenbau Scholz GmbH & Co. KG/steam generator: WIMA ED36). The autoclave was programed as follows: 20 min vacuum (−0.8 bar), heating up to 187 °C/11 bar within 1.5 h, holding a plateau of 187 °C/11 bar for 5 h, cooling down to 0 bar within 1.5 h. After this procedure, at least 5 cm of each side of the sample were removed by band saw in order to obtain an undisturbed pore structure (eliminating the “wall-effect”).

2.3. Characterization

2.3.1. Green body

Before the mix was cast, the spread flow was tested by completely filling a cone (diameter d_{cone}=7 cm, height h_{cone}=6 cm, volume V_{cone}=244 ml) and then measuring the diameter of the resulted cake on the glass plate after the vertical removal of the cone. After mixing, the slurry was immediately cast in insulated moulds (XPS with parting agent, 27 l in volume, semi-calorimetric environment) and the temperature and rising behaviour were recorded using a data logger as shown in Fig. 2. The stiffening was determined by a special indenter (pointy cone, mass=30 g) placed vertically on the surface of the mass, which can penetrate the mass by its own weight. The penetration depth of the cone in time is a measure of the stiffness of the mix (similar to the determination of setting time using a Vicat needle setup). When the penetration depth reaches less than 20 mm, the measurement stops.

2.3.2. Hardened state analyse

The prepared material was cut in cubes (100×100×100 mm^3) for raw density (or apparent density) and compressive strength measurements. The polished cubes were oven dried (60 °C, forced ventilation) until constant weight. After cooling down to 20 °C, the raw density ϱ_{AAC} and the compressive strength σ (FORM+TEST Seidner+Co. GmbH, MEGA 110-200 D-S) were measured. The approach is comparable to the standards EN 771-4 [43] and EN 772 [44]. The thermal conductivity λ was measured using an ISOMET model 2104 device (Applied Precision), by measuring multiple times on a polished surface.

A microscopic analysis of the powders was performed using a Scanning Electron Microscope (SEM). The phase composition was measured using an X-Ray Diffractometer (XRD, PANalytical X'Pert PRO MPD with CuK_α radiation and an X'Celerator RTMS detector with back loading preparation, 20 mm sample diameter, 15 mm irradiated sample length, 5–90° 2θ, 0.02° 2θ/step, 41.3 s/step, variable slits, 40 mA, 45 kV). The drying shrinkage was determined according to RILEM AAC5.2. The samples were firstly immersed in water for 72 h for saturation and then the first length within 30 min after removing from the water was measured. The drying shrinkage and mass of the samples were measured while the samples were placed in a chamber at a temperature of 20 ± 2 °C and humidity of 43 ± 2% (controlled by K_2CO_3). After reaching the constant length, all samples were dried in an oven at 105 °C until constant masses were attained and then the moisture contents of individual samples were determined.

3. Results and discussion

3.1. Mix design

In previous research [6], the parameters that can affect the final properties of AAC were studied, including the water-to-solid ratio and foaming agent content. In the present study, water to solid ratio of 0.625 and metallic Al powder content of 0.083% were chosen for the preparation of normal AAC as reference samples.

First of all, the target flowability (spread flow 25 ± 3 cm [6]) should be achieved when fully replacing cement by sodium carbonate activated slag. In general, the sodium carbonate dosage, water-to-solid ratio, the water temperature and sequence of raw materials addition should be

considered. Different from what has been observed for the production of ordinary concrete on the strength development, the water-to-solid ratio mainly influences the viscosity of the mixture and consequently the pore size and distribution of AAC. In this case, the main parameters studied were the other three factors. Considering the reactivity of the raw materials and intensity of the reaction, the sequence of preparing the mixture was determined based on preliminary experiments, as shown in Fig. 2.

The preparation of cement-based AAC normally uses a pre-heated water (≈45 °C), which can benefit the hydration of free lime and cement, leading to a faster strength development and stiffness of the green body [45]. However, the preliminary study shows that the high temperature water may not be suitable for the preparation of ASAAC as the reaction was too fast and uncontrollable when adding the reactive materials such as CaO and slag, leading to a low flowability and unevenly mixed product. In this case, tap water (20 °C) was applied in the present study.

The dosage of sodium carbonate (expressed as equivalent Na_2O wt %) was calculated by the mass of slag. To ensure the mechanical properties of the reaction product, dosages of sodium carbonate between 4 and 8 Na_2O wt% by mass of slag were chosen and the water to solid ratio was kept the same as the reference. However, the produced alkali activated materials were too viscous, which leads to a poor spread flow. In fact, the high viscosity is normally found in alkali activated materials, probably due to the fast reaction of the slag particles in alkaline environment [46–48]. In the ASAAC system, the precipitation of calcium carbonate also negatively influences the flowability when mixing sodium carbonate solution with portlandite because the increased pH (Eq. (2)) will limit the solubility of $Ca(OH)_2$. When adding slag at the stage II, the high pH will also lead to the fast reaction generating strength-giving phases, e.g. calcium silicate hydrates, which will also reversely influence the workability, demanding more water to reach the target flowability. As a result, a higher amount of water was required and the water to solid ratio was finally chosen to be 0.7, based on the performed experiments. Considering the dilution effect, a higher alkali dosage (6%) was applied. Fig. 3 shows the spread flow of samples. As can be seen, by properly changing the mixing parameters, the target flowability was achieved. It should be noted that a higher dosage of sodium carbonate was also studied and the target flowability and green hardening was reached. However, the reaction of Al powder started too fast under this condition which made the mixing process very hard to control (not shown here). Thus, the designed mixture (Table 2) was selected for further investigation.

3.2. Green body development

The green body development is an important parameter that determines the material properties of the produced product. After

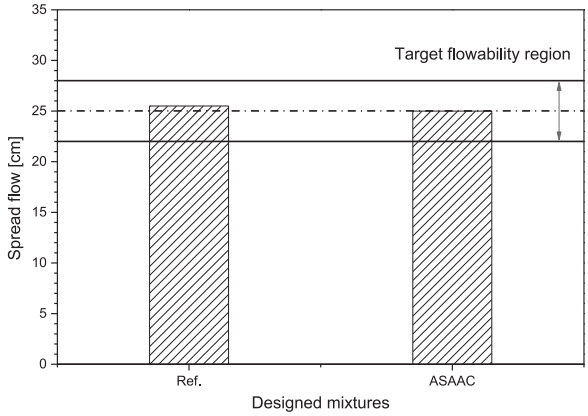

Fig. 3. Flowability of prepared AAC and ASAAC.

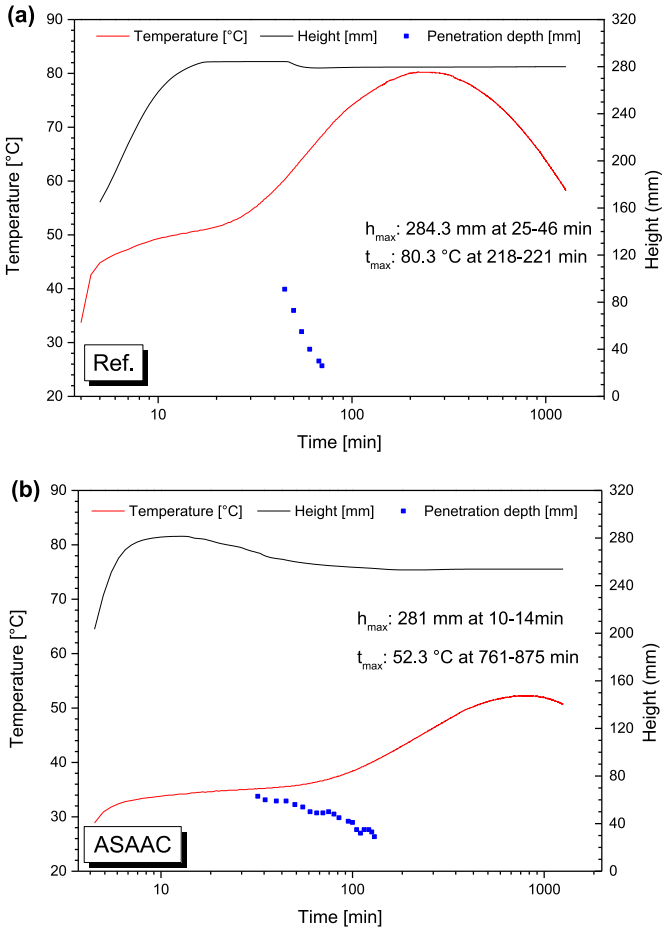

Fig. 4. Green body development parameters of (a) AAC and (b) ASAAC, including temperature, rising height and penetration depth.

mixing and casting, the temperature, rising height and penetration depth during the green body development were measured, using the device depicted in Fig. 2. Due to the device limits, the data were only recorded when the samples triggered the initial measuring conditions, i.e. rising height was measured when the sample raised to around 60 mm. As can be seen in Fig. 4, the reference AAC reached the maximum height (284 mm, upper limit of the device) at approximate 25 min after mixing, while ASAAC required much less time (about 10 min) due to the high pH environment, indicating a faster reaction (Eq. (1)). Though the rising rate of ASAAC is much faster than that of the reference AAC, the stiffening of the green body is slower. As a result, in turn, a sharp drop happened in the ASAAC mixture as the matrix was not strong enough to support its own weight after the emission of H_2 gas from the matrix.

On the other hand, the temperature rising process can generally be classified into two steps (Fig. 4). The first step is normally the initial reaction of Al powder, while the hydration of free lime and cement/alkali activated material is responsible for the second step. In overall, the maximum temperature and rising rate of the green body of ASAAC are lower than the reference AAC. The maximum temperature of ASAAC (52.3 °C) occurred after 761 min of mixing, while the reference sample happened much earlier at 218 min with a higher maximum temperature of 80.3 °C. According to Arrhenius equation, under the similar condition the temperature is the main driving force of the reaction. In this case, the initial temperature of the tap water can partly be responsible for the reduced intensity and delayed reaction of free lime and alkali activated materials.

The penetration depth can give an indication about the stiffness and the strength development of the green body. It is clear that the initial

Table 3
Apparent density and compressive strength of the mixtures.

Mixtures unit	Apparent density [kg/m^3]	Compressive strength [MPa]
Ref.	455 ± 4.4	3.27 ± 0.06
ASAAC	538 ± 4.1	2.42 ± 0.14

Table 4
True density, porosity and thermal conductivity of the specimens.

Mixtures unit	True density [g/cm^3]	Porosity [%]	Thermal conductivity [W/(m K)]
Ref.	2.60	82.5	0.082 ± 0.001
ASAAC	2.51	78.6	0.093 ± 0.001

stiffness of ASAAC happened slightly earlier than AAC, however, while its strength development was slower by giving a gentle decrease on the penetration depth. The stiffness process is also largely correlated to the rising height results. After reaching the maximum rising height, in the meantime H_2 gas has been gradually emitted, and the green body started setting until reaching the minimum stiffness supporting its own weight. It is clear that these three parameters, temperature, rising height and penetration depth, are highly correlated to each other, determining the properties of the produced products as a result.

3.3. Hardened state characterization

After autoclaving, cutting and polishing, the apparent density and compressive strength of the samples were determined, as shown in Table 3. It is clear that the apparent density of the ASAAC (538 kg/m^3) is slightly higher than that of the reference AAC (455 kg/m^3), while the strength is lower (2.42 MPa compared to 3.27 MPa). In general, the strength development is inversely proportional to the porosity of autoclaved aerated concrete [49]. However, the shape, size and distribution of pores also significantly affect the mechanical properties of samples. Fig. 5 show the pore structure of both ASAAC and reference samples. As can be seen, the pores of the produced ASAAC sample have a preferred orientation as expressed by their elliptical shape, while the AAC mixture shows spherical and well distributed pores. The preferred orientation of the pore can be the consequence of the collapse happened at around 14–160 min (Fig. 4), leading to a poor structure with a reduced load bearing capacity. This pore structure and its disturbance might be as well a result of the changed bulk chemistry (the CaO/SiO_2-mass ratio changed from 0.35 to 0.25).

Table 4 presents the physical properties of the synthesized mixtures, including the true density, porosity and thermal conductivity. A similar true density is observed for samples prepared by alkali activation compared to the reference samples, indicating a similar phase composition and the porosity of ASAAC is only 4.7% lower than reference. The thermal conductivity of the alkali activated samples is slightly higher than the reference. Schauerte and Trettin [50] reported that the thermal conductivity is mainly controlled by the macrospores while the influence of small pores such as microspores and mesopores are not prominent, which is also confirmed by Yu et al. [51]. As a result, the slightly lower porosity of ASAAC could cause the higher thermal conductivity. Nevertheless, it is notable that the thermal conductivity of all samples remains at a similar level. Kunchariyakun et al. [9] prepared autoclaved aerated concretes incorporating rice husk ash and reported the lowest thermal conductivity of 0.267 W/(m K) with the unit weight of 671 kg/m^3. Rozycka and Pichor [52] investigated the effect of perlite waste addition on the properties of autoclaved aerated concrete and found a thermal conductivity coefficient of 0.110–0.127 W/(m K) when the bulk density is around 480–650 kg/m^3. According to literatures [7,53], the typical thermal conductivity range (3% moisture) of samples with dry density of 450–600 kg/m^3 is 0.12–0.16 W/(m K). It should be noted that the thermal conductivity is not only determined by the porosity related parameters, but also can be significantly affected by the moisture content and the phase composition [7,54–56]. However, in this case, the influence of these factors is not prominent due to the fact that both samples were measured under the same conditions and the difference of the values is more prominent than the value itself.

Fig. 6 presents the drying shrinkage of samples as a function of the moisture content. As can be seen, the drying shrinkage of ASAAC is rather similar to that of the reference AAC by giving a slightly higher total drying shrinkage and moisture content of the samples. However, it should be noted that the drying shrinkage of the reference AAC is relatively high, probably due to the special raw material combination, compared to commercial AAC products (max. 0.4 mm/m) according to EN 12602 [57]. In general, the shrinkage is mainly affected by the content of amorphous phases (C-S-H gel) while the effect of crystalline phases (tobermorite) is not prominent, which will be discussed later with the microstructure analysis. Besides, the pore structure can also influence the shrinkage. Georgiades et al. [58] concluded that the drying shrinkage is significantly affected by the smallest pore size (20–200 Å) because of a change in disjoining pressure. Alkali activated materials have been reported to contain high amount of mirco-pores which lead to a high drying shrinkage [59]. Aydın and Baradan [60] also concluded that the incorporation of alkali cations in C-A-S-H leads to a large shrinkage. However, they also mentioned that the shrinkage can be substantially reduced by autoclaving curing which shows equal level to cement based sample. In this case, the slightly higher shrinkage of ASAAC samples could be attributed to the slight microstructure differences induced by the incorporation of the alkali activator. Nevertheless, the difference is relatively small, indicating a similar microstructure.

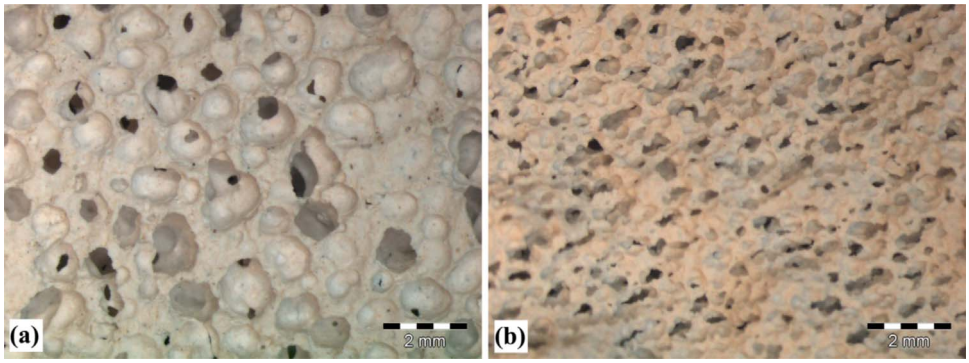

Fig. 5. Pictures of pore structure of (a) AAC and (b) ASAAC.

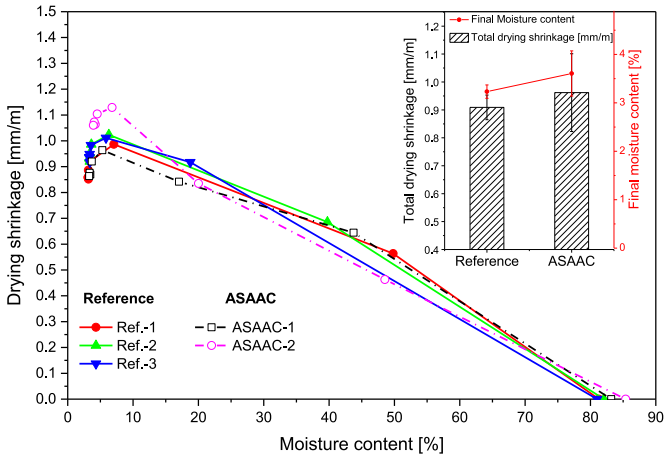

Fig. 6. Shrinkages of 3 AAC samples and 2 ASAAC samples as a function of moisture content (Shrinkage is highly related to moisture content of individual samples).

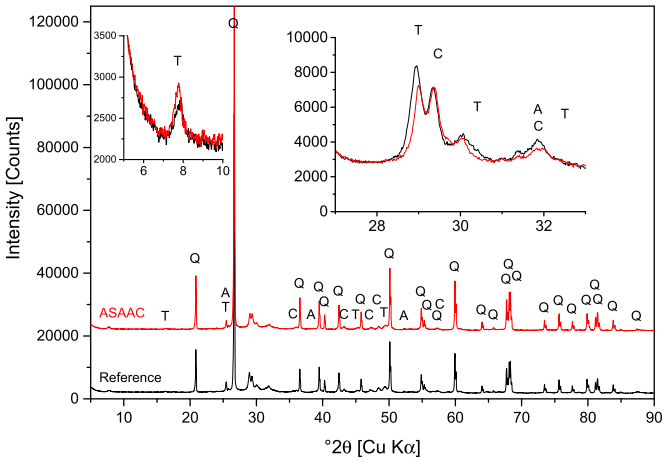

Fig. 8. XRD patterns of AAC and ASAAC (T – Tobermorite, C – Calcite, A – Anhydrite, Q – Quartz).

3.4. Microstructure and phase analysis

Fig. 7 presents the SEM pictures of ASAAC with different sodium carbonate dosages (4, 6 and 8 Na_2O wt%) and reference AAC. As can be seen, in both cases, the main binding phase of autoclaved aerated samples is tobermorite. A good way to observe the quality of tobermorite is to investigate the shape of the crystals in the pores, where they could grow freely in space [3,61,62]. In general, the crystals have a platy shape. The reference AAC sample (Fig. 7a) however shows tobermorite with a more needle shaped character, so more towards the C-S-H (I) gel than the crystalline modification. This is most likely caused by a very pure and fine quartz powder, so the solubility of SiO_2 is too high [62]. However, in the case of the alkali activation, the shape of the crystals is highly depending on the sodium carbonate dosage. Similar crystallinity is observed for the mixture with 4% sodium carbonate dosage (Fig. 7b) and more sword like which means more close towards optimal, i.e. crystalline structure of C-S-H gel is observed when the dosage of Na_2CO_3 is 6% (Fig. 7c). However, further increasing the alkali dosage leads to a poor crystallinity (Fig. 7d), indicating that the optimal sodium carbonate dosage on the crystallinity of the reaction product is close to 6%. As well no changes in the matrix between the reference and the alkali activated sample could be observed. Alexanderson [49] found that the shrinkage decreased with the increasing crystallinity, which is defined as the percentage of 11.3 Å tobermorite out of the total amount of calcium silicate hydrates. In this case, the slightly higher drying shrinkage of ASAAC can be mainly attributed to the weakened pore structure.

The X-ray diffraction results are shown in Fig. 8. It is clear that the incorporation of 6% sodium carbonate does not change the main reaction product, which is tobermorite. However, a slight change on the chain of tobermorite is observed for ASAAC samples by giving a shift from position 11.25 toward 11.38 Å, indicating a higher incorporation of Al in the chain of tobermorite [63,64]. Moreover, the intensity of the tobermorite at 11.3 Å (7.7°2θ) and 3.085 Å (28.9°2θ) also differs due to different preferred orientations of the different shape of the crystals. The shape indicates a more plate like appearance, which is favourable

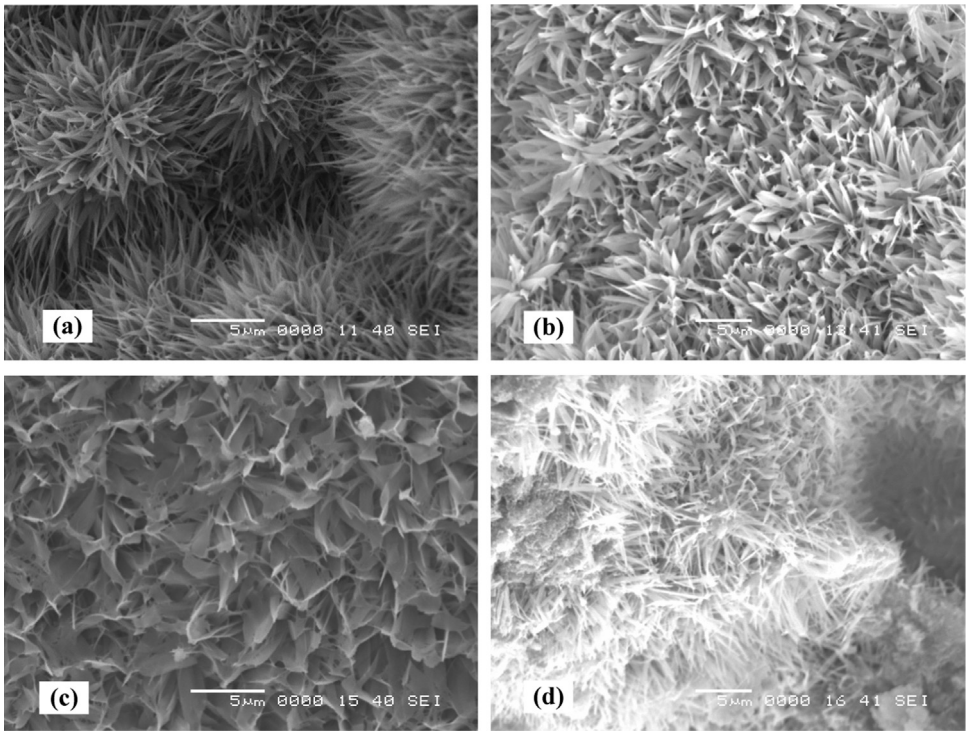

Fig. 7. SEM pictures of broken samples of (a) AAC and ASAAC with sodium carbonate dosages of (b) 4%, (c) 6% and (d) 8%.

for AAC physical properties (strength and shrinkage), which is consistent with the SEM results (Fig. 7). Besides, the small shift at ≈3.085 Å (28.9°2θ) could be caused by the incorporation of alkalis in the chain of calcium silicate hydrates [63,64]. This is in coherence with the natural tobermorite and related natural C-S-H phases, which always show some alkali and aluminium incorporation [61,65]. From this point of view a coupled substitution of (Al^{3+}+Na^{+}) and Si^{4+} might be considered. Nevertheless, the reaction products of ASAAC and the reference AAC are the same, which is also consistent with the other experimental results that the properties are similar.

3.5. Cost and environmental analyses

AAC product has been used more and more in practical constructions. As analyzed above, most of properties of the produced ASAAC product are comparable to the reference samples, indicating that the alkali activated material is suitable for the purpose of this application. However, to attract interests from the commercial market, not only the material properties but also the cost related issues should be considered. Sodium carbonate and slag were used to replace cement in the investigated mixtures, while all other ingredients and technical parameters (e.g. autoclaving/steaming process) were kept the same. It would be reliable to compare the entire system, including the cost and environmental impact of all raw materials and involved technological process in the calculation. However, the system is very complex that it is extremely hard to retrieve all comparable sources for the cost, energy consumption and CO_2 emission involved in the production, treatment and transportation, etc. Besides, the database differs from country to country and company to company, which leads the possible calculated results open for discussion. In this case, a simplified calculation is preferred for comparison purpose, due to the fact that the main differences between the two mixtures are cement and sodium carbonate with slag. Moseson et al. [32] have performed a life cycle assessment on the cement production and sodium carbonate activated slag, which is used as an input source for the calculation in the present study.

Table 5 presents the calculated results of the cost, energy consumption and CO_2 emission of preparing sodium carbonate activated slag compared to the production of cement per ton. As can be seen, the cost and energy consumption are reduced 19.3% and 91.3% after replacing cement with alkali activated material, respectively. Due to the low content of sodium carbonate, the cost is highly depending on the local price of GGBS. As the sodium carbonate is normally received as powder and then dissolved in water prior to preparation, the cost and environmental impacts can be further reduced by reducing the thermal treatment when producing sodium carbonate. Moreover, it is remarkable to notice that a reduction of 97.6% on the CO_2 emission is achieved. It should be noted that the calculated results only compared the production of cement and sodium carbonate activated slag, while, the reductions will be much lower if the whole production process of all materials is considered.

In previous studies, comparable properties of aerated concretes using activators of waterglass modified by sodium hydroxide were also achieved [14,16,47]. However, the production was relatively expensive due to the higher cost of waterglass which accounts for 80% of the total cost. By applying sodium carbonate as the activator, the cost can be lower than OPC based reference sample and the energy consumption and CO_2 emission are also reduced, which will render the product even more competitive. However, it should be noted that the utilization of ground granulated blast furnace slag in producing AAC could potentially raise challenges to the manufacture, e.g. the production process releases H_2S which can cause corrosion to the equipment and additional ventilation is therefore needed.

Table 5
Life cycle assessment of the mixtures produced with cement and sodium carbonate activated slag (* an exchange rate 0.95 of $ to € was applied [32]).

Mixtures	Cost* €	CO_2 emission kg	Energy consumption kW h
Cement (ton)	96.9	1510.2	896.7
Sodium carbonate activated GGBS (ton)	78.2	36.5	77.8
Sodium carbonate (0.094 t)	9.3	10.4	35.1
GGBS (0.906 t)	68.9	26.1	42.8
Reduction	19.3%	97.6%	91.3%

4. Conclusion

This study investigated the sodium carbonate activated slag to replace cement in autoclaved aerated concrete (AAC), named alkali activated autoclaved aerated concrete (ASAAC). The produced ASAAC product shows comparable properties or better performance to the reference samples with respect to porosity, drying shrinkage, strength development, cost and environmental impact. Besides, from the microstructure point of view, the crystallinity of the product is higher than the reference sample. The principle of a cement free alkali activated AAC was successfully tested. Based on the experiments, the following conclusions can be drawn:

1. A higher incorporation of Al and alkalis (Na) in the chain of tobermorite is observed for ASAAC sample.
2. The crystallinity of ASAAC is better than in the reference AAC when the dosage of sodium carbonate is low (≈6%), while further increasing the sodium carbonate dosage leads to a poorer crystallinity.
3. The shrinkage of ASAAC is similar to the reference AAC samples, regardless of the fact that shrinkage of the reference AAC is high probably due to the fine quartz applied.
4. The ASAAC shows very good thermal properties, indicated by the thermal conductivity of 0.093 W/(m K).
5. The ASAAC possess a relatively poor strength (2.42 MPa), which can be further improved in future by more in depth study of the system, e.g. a better controlled pore structure or an adjustment of the bulk chemistry.
6. The new ASAAC provides significant benefits with respect to cost reduction and environmental impact.

Acknowledgements

This research was carried out under the scheme of China Scholarship Council, Eindhoven University of Technology and the frame work of the Research Program of the Materials Innovation Institute M2i (www.m2i.nl), Project number M81.6.12478, together with the industrial partner HESS AAC systems B.V. The authors highly appreciate the remarks and the advice of Mr. Ladislaus Heinz. Many thanks as well are given to Knauf Gips KG, Holcim (Deutschland) AG, Fels-Werke GmbH and Enci B.V. for supplying materials, and Tata Steel for using their SEM, as well as to the Fachgruppe Mineralogie/Geochemie from Martin-Luther Universität Halle-Wittenberg (Germany) for the use of their XRD. Furthermore, the authors wish to express their gratitude to the following sponsors of the Building Materials research group at TU Eindhoven: Rijkswaterstaat Grote Projecten en Onderhoud, Graniet-Import Benelux, Kijlstra Betonmortel, Struyk Verwo, Attero, Rijkswaterstaat Zee en Delta - District Noord, Van Gansewinkel Minerals, BTE, V.d. Bosch Beton, Selor, GMB, Icopal, BN International, Eltomation, Knauf Gips, Kronos, Joma, CRH Europe Sustainable Concrete Centre, Cement & BetonCentrum, Heros, Inashco, Keim, Sirius International, Boskalis and NNERGY.

References

[1] N. Narayanan, K. Ramamurthy, Structure and properties of aerated concrete: a review, Cem. Concr. Compos. 22 (2000) 321–329. http://dx.doi.org/10.1016/S0958-9465(00)00016-0.

[2] E.C. Pytlik, J. Saxena, Advances in autoclaved aerated concrete, in: Proceedings 3rd RILEM International Symposium Autoclaved Aerated Concrete, 1992, p. 18.

[3] S.G. Zürn, E. der Sandminerale, auf die Bildung von Calciumsilikathydraten (CSH-Phasen), das Gefüge und die mechanischen Eigenschaften von Porenbetonprodukten Systematische Untersuchungen an synthetischen Sandmischungen mit Übertragung auf Produktionssande, Logos Verlag, Berlin, Germany, 1997.

[4] S. Reinsdorf, L. II Porenbetone, VEB Verlag für Bauwesen, Berlin, Germany, 1963.

[5] B. Walk-Lauffer, Untersuchung des Einflusses von Sulfaten auf das System CaO-SiO2-Al2O3-K2O-H2O mittels Wärmeflusskalorimetrie und in-situ Neutronenbeugung unter hydrothermalen Bedingungen, Universität Siegen, 2002.

[6] C. Straub, M.V.A. Florea, H.J.H. Brouwers, Autoclaved aerated concrete – mix parameters and their influence on final properties, in: 19. International Baustofftagung, 2015, pp. 2822–2829.

[7] A.J. Hamad, Materials, production, properties and application of aerated lightweight concrete: review, Int. J. Mater. Sci. Eng. 2 (2014) 152–157. http://dx.doi.org/10.12720/ijmse.2.2.152-157.

[8] X. Huang, W. Ni, W. Cui, Z. Wang, L. Zhu, Preparation of autoclaved aerated concrete using copper tailings and blast furnace slag, Constr. Build. Mater. 27 (2012) 1–5. http://dx.doi.org/10.1016/j.conbuildmat.2011.08.034.

[9] K. Kunchariyakun, S. Asavapisit, K. Sombatsompop, Properties of autoclaved aerated concrete incorporating rice husk ash as partial replacement for fine aggregate, Cem. Concr. Compos. 55 (2015) 11–16. http://dx.doi.org/10.1016/j.cemconcomp.2014.07.021.

[10] A. Hauser, U. Eggenberger, T. Mumenthaler, Fly ash from cellulose industry as secondary raw material in autoclaved aerated concrete, Cem. Concr. Res. 29 (1999) 297–302. http://dx.doi.org/10.1016/S0008-8846(98)00207-5.

[11] H. Kurama, I.B. Topçu, C. Karakurt, Properties of the autoclaved aerated concrete produced from coal bottom ash, J. Mater. Process. Technol. 209 (2009) 767–773. http://dx.doi.org/10.1016/j.jmatprotec.2008.02.044.

[12] X.Y. Cong, S. Lu, Y. Yao, Z. Wang, Fabrication and characterization of self-ignition coal gangue autoclaved aerated concrete, Mater. Des. 97 (2016) 155–162. http://dx.doi.org/10.1016/j.matdes.2016.02.068.

[13] F. Pacheco-Torgal, J. Castro-Gomes, S. Jalali, Alkali-activated binders: a review, Constr. Build. Mater. 22 (2008) 1305–1314. http://dx.doi.org/10.1016/j.conbuildmat.2007.10.015.

[14] Z. Zhang, J.L. Provis, A. Reid, H. Wang, Geopolymer foam concrete: an emerging material for sustainable construction, Constr. Build. Mater. 56 (2014) 113–127. http://dx.doi.org/10.1016/j.conbuildmat.2014.01.081.

[15] Z. Zhang, J.L. Provis, A. Reid, H. Wang, Mechanical, thermal insulation, thermal resistance and acoustic absorption properties of geopolymer foam concrete, Cem. Concr. Compos. 62 (2015) 97–105. http://dx.doi.org/10.1016/j.cemconcomp.2015.03.013.

[16] Z. Abdollahnejad, F. Pacheco-Torgal, T. Felix, W. Tahri, J. Barroso Aguiar, Mix design, properties and cost analysis of fly ash-based geopolymer foam, Constr. Build. Mater. 80 (2015) 18–30. http://dx.doi.org/10.1016/j.conbuildmat.2015.01.063.

[17] H. Esmaily, H. Nuranian, Non-autoclaved high strength cellular concrete from alkali activated slag, Constr. Build. Mater. 26 (2012) 200–206. http://dx.doi.org/10.1016/j.conbuildmat.2011.06.010.

[18] A.F. Jimenez, F. Puertas, Setting of alkali-activated slag cement. Influence of activator nature, Adv. Cem. Res. 13 (2001) 115–121. http://dx.doi.org/10.1680/adcr.2001.13.3.115.

[19] F. Puertas, A.F. Jimenez, M.T. Blanco-Varela, Pore solution in alkali-activated slag cement pastes. Relation to the composition and structure of calcium silicate hydrate, Cem. Concr. Res. 34 (2004) 139–148. http://dx.doi.org/10.1016/S0008-8846(03)00254-0.

[20] M. Komljenovic, Z. Bascarevic, V. Bradic, Mechanical and microstructural properties of alkali-activated fly ash geopolymers, J. Hazard. Mater. 181 (2010) 35–42. http://dx.doi.org/10.1016/j.jhazmat.2010.04.064.

[21] F. Pacheco-Torgal, J.A. Labrincha, C. Leonelli, A. Palomo, P. Chindaprasirt, Handbook of Alkali-activated Cement, Mortars and Concretes, 2015.

[22] J.L. Provis, J.S.J. Van Deventer, Alkali Activated Materials. http://dx.doi.org/10.1007/978-94-007-7672-2, 2014.

[23] S. Wang, K.L. Scrivener, P.L. Pratt, Factors affecting the strength of alkali-activated slag, Cem. Concr. Res. 24 (1994) 1033–1043.

[24] T. Bakharev, J.G. Sanjayan, Y.B. Cheng, Alkali activation of Australian slag cements, Cem. Concr. Res. 29 (1999) 113–120. http://dx.doi.org/10.1016/S0008-8846(98)00170-7.

[25] X. Gao, Q.L. Yu, H.J.H. Brouwers, Characterization of alkali activated slag–fly ash blends containing nano-silica, Constr. Build. Mater. 98 (2015) 397–406. http://dx.doi.org/10.1016/j.conbuildmat.2015.08.086.

[26] X. Gao, Q.L.L. Yu, H.J.H.J.H. Brouwers, Reaction kinetics, gel character and strength of ambient temperature cured alkali activated slag-fly ash blends, Constr. Build. Mater. 80 (2015) 105–115. http://dx.doi.org/10.1016/j.conbuildmat.2015.01.065.

[27] A.R. Brough, A. Atkinson, Sodium silicate-based, alkali-activated slag mortars Part I. Strength, hydration and microstructure, Cem. Concr. Res. 32 (2002) 865–879.

[28] A.R. Brough, M. Holloway, J. Sykes, A. Atkinson, Sodium silicate-based alkali-activated slag mortars Part II. The retarding effect of additions of sodium chloride or malic acid, Cem. Concr. Res. 30 (2000) 1375–1379.

[29] A.M. Rashad, A comprehensive overview about the influence of different additives on the properties of alkali-activated slag – a guide for civil engineer, Constr. Build. Mater. 47 (2013) 29–55. http://dx.doi.org/10.1016/j.conbuildmat.2013.04.011.

[30] D.M. Roy, Alkali-activated cements opportunities and challenges, Cem. Concr. Res. 29 (1999) 249–254. http://dx.doi.org/10.1016/S0008-8846(98)00093-3.

[31] N.N. Greenwood, A. Earnshaw, Chemistry of the Elements, 2nd ed., Butterworth-Heinemann, United Kingdom, 1997.

[32] A.J. Moseson, D.E. Moseson, M.W. Barsoum, High volume limestone alkali-activated cement developed by design of experiment, Cem. Concr. Compos. 34 (2012) 328–336. http://dx.doi.org/10.1016/j.cemconcomp.2011.11.004.

[33] B. Yuan, Q.L. Yu, H.J.H. Brouwers, Reaction kinetics, reaction products and compressive strength of ternary activators activated slag designed by Taguchi method, Mater. Des. 86 (2015) 878–886. http://dx.doi.org/10.1016/j.matdes.2015.07.077.

[34] S.A. Bernal, J.L. Provis, R.J. Myers, R. San Nicolas, J.S.J. van Deventer, Role of carbonates in the chemical evolution of sodium carbonate-activated slag binders, Mater. Struct. 48 (2014) 517–529. http://dx.doi.org/10.1617/s11527-014-0412-6.

[35] T. Bakharev, J.G. Sanjayan, Y.B. Cheng, Effect of admixtures on properties of alkali-activated slag concrete, Cem. Concr. Res. 30 (2000) 1367–1374. http://dx.doi.org/10.1016/S0008-8846(00)00349-5.

[36] F. Puertas, M.T. Carrasco, Use of glass waste as an activator in the preparation of alkali-activated slag. Mechanical strength and paste characterisation, Cem. Concr. Res. 57 (2014) 95–104. http://dx.doi.org/10.1016/j.cemconres.2013.12.005.

[37] X. Ke, S.A. Bernal, J.L. Provis, Controlling the reaction kinetics of sodium carbonate-activated slag cements using calcined layered double hydroxides, Cem. Concr. Res. 81 (2016) 24–37. http://dx.doi.org/10.1016/j.cemconres.2015.11.012.

[38] A.F. Abdalqader, F. Jin, A. Al-Tabbaa, Characterisation of reactive magnesia and sodium carbonate-activated fly ash/slag paste blends, Constr. Build. Mater. 93 (2015) 506–513. http://dx.doi.org/10.1016/j.conbuildmat.2015.06.015.

[39] M. Kovtun, E.P. Kearsley, J. Shekhovtsova, Chemical acceleration of a neutral granulated blast-furnace slag activated by sodium carbonate, Cem. Concr. Res. 72 (2015) 1–9. http://dx.doi.org/10.1016/j.cemconres.2015.02.014.

[40] H. Kuhl, Slag Cement and Process of Making the Same, 1908.

[41] J.A. Eriksson, V. zur Herstellung, von poroesen Baustuecken aus Beton, DE 447194C, 1924.

[42] J.A.H. Oates, Lime and Limestone Chemistry and Technology, Production and Uses, Wiley-VCH Verlag GmbH, Weinheim, Germany, 1998.

[43] DIN EN 771-4, Berlin, Germany, 2003.

[44] DIN EN 772, Berlin, Germany, n.d.

[45] C.L. Wang, W. Ni, S.Q. Zhang, S. Wang, G.S. Gai, W.K. Wang, Preparation and properties of autoclaved aerated concrete using coal gangue and iron ore tailings, Constr. Build. Mater. 104 (2016) 109–115. http://dx.doi.org/10.1016/j.conbuildmat.2015.12.041.

[46] C. Shi, D. Roy, P. Krivenko, Alkali-Activated Cements and Concretes, CRC Press, USA, 2005.

[47] B. Singh, G. Ishwarya, M. Gupta, S.K. Bhattacharyya, Geopolymer concrete: a review of some recent developments, Constr. Build. Mater. 85 (2015) 78–90. http://dx.doi.org/10.1016/j.conbuildmat.2015.03.036.

[48] B. Yuan, Q.L. Yu, H.J.H. Brouwers, Evaluation of slag characteristics on the reaction kinetics and mechanical properties of Na2CO3 activated slag, Constr. Build. Mater. 131 (2017) 334–346. http://dx.doi.org/10.1016/j.conbuildmat.2016.11.074.

[49] J. Alexanderson, Relations between structure and mechanical properties of autoclaved aerated concrete, Cem. Concr. Res. 9 (1979) 507–514. http://dx.doi.org/10.1016/0008-8846(79)90049-8.

[50] M. Schauerte, R. Trettin, Schaumbetonherstellung auf der Grundlage von Ultrahochleistungsbeton (UHPC), in: GDCh Tagungsband Tagung Bauchemie, Hamburg, 2011, pp. 140–146.

[51] Q.L. Yu, P. Spiesz, H.J.H. Brouwers, Ultra-lightweight concrete: conceptual design and performance evaluation, Cem. Concr. Compos. 61 (2015) 18–28. http://dx.doi.org/10.1016/j.cemconcomp.2015.04.012.

[52] A. Różycka, W. Pichór, Effect of perlite waste addition on the properties of autoclaved aerated concrete, Constr. Build. Mater. 120 (2016) 65–71. http://dx.doi.org/10.1016/j.conbuildmat.2016.05.019.

[53] J. Newman, B.S. Choo, P. Owens, Advanced Concrete Technology 3: Processes, Elsevier Ltd, UK, 2003.

[54] Q.L. Yu, P. Spiesz, H.J.H. Brouwers, Development of cement-based lightweight composites – Part 1: mix design methodology and hardened properties, Cem. Concr. Compos. 44 (2013) 17–29. http://dx.doi.org/10.1016/j.cemconcomp.2013.03.030.

[55] Q.L. Yu, H.J.H. Brouwers, Development of a self-compacting gypsum-based lightweight composite, Cem. Concr. Compos. 34 (2012) 1033–1043. http://dx.doi.org/10.1016/j.cemconcomp.2012.05.004.

[56] D.M.A. Huiskes, A. Keulen, Q.L. Yu, H.J.H. Brouwers, Design and performance evaluation of ultra-lightweight geopolymer concrete, Jmade 89 (2015) 516–526. http://dx.doi.org/10.1016/j.matdes.2015.09.167.

[57] EN 12602-2008, Prefabricated Reinforced Components of Autoclaved Aerated Concrete, n.d.

[58] A. Georgiades, C. Ftikos, J. Marinos, Effect of micropore structure on autoclaved aerated concrete shrinkage, Cem. Concr. Res. 21 (1991) 655–662. http://dx.doi.org/10.1016/0008-8846(91)90116-Y.

[59] H. Ye, A. Radlinska, Shrinkage mechanisms of alkali-activated slag, Cem. Concr. Res. 88 (2016) 126–135. http://dx.doi.org/10.1016/j.cemconres.2016.07.001.

[60] S. Aydın, B. Baradan, Mechanical and microstructural properties of heat cured alkali-activated slag mortars, Mater. Des. 35 (2012) 374–383. http://dx.doi.org/

10.1016/j.matdes.2011.10.005.
[61] K. Garbev, Struktur, Eigenschaften und quantitative Rietveldanalyse von hydrothermal kristallisierten Calciumsilikathydraten (C-S-H-Phasen), Forschungszentrum Karlsruhe in der Helmholtz-Gemeinschaft, 2004.
[62] H. Poellmann, G. Schober, J. Scarbath, Investigations on phase development in autoclaved calcium silicate building products (autoclaved aerated concrete), in: Proceedings of the 21st International Conference Cem. Microsocopy, 1999, pp. 284–305.
[63] S. Komarneni, R. Roy, D.M. Roy, C.A. Fyfe, G.J. Kennedy, A.A. Bothner-By, J. Dadok, A.S. Chesnick, 27Al and 29Si magic angle spinning nuclear magnetic resonance spectroscopy of Al-substituted tobermorites, J. Mater. Sci. 20 (1985) 4209–4214. http://dx.doi.org/10.1007/BF00552416.
[64] M. Tsuji, S. Komarneni, P. Malla, Substituted tobermorites: 27Al and 29Si MASNMR, cation exchange, and water sorption studies, J. Am. Ceram. Soc. 74 (1991) 274–279. http://dx.doi.org/10.1111/j.1151-2916.1991.tb06874.x.
[65] Heddle, Preliminary notice of substances which may prove to be new minerals, Miner. Mag. 4 (1880) 117–123.